Appl Nanosci (2016) 6:387–397
DOI 10.1007/s13204-015-0450-6

ORIGINAL ARTICLE

Highly oriented and physical properties of sprayed anatase Sn-doped TiO_2 thin films with an enhanced antibacterial activity

S. Dhanapandian[1] · A. Arunachalam[1] · C. Manoharan[1]

Received: 27 February 2015 / Accepted: 12 April 2015 / Published online: 28 April 2015

Abstract Pristine TiO_2 and Sn-doped TiO_2 thin films with different Sn doping levels (2, 4, 6 and 8 at.%) were deposited by employing a simplified spray pyrolysis technique. The XRD pattern of the films confirmed tetragonal structure with the polycrystalline nature. The films exhibited a pure anatase titanium dioxide (TiO_2) with a strong orientation along (101) plane. The scanning electron microscopy image of 6 at.% Sn-doped TiO_2 thin film depicted nanosized grains with porous nature. The atomic force microscopy study had shown the columnar arrangement of grains with the increase in particle size and surface roughness for 6 at.% Sn-doped TiO_2 thin films. The optical transmittance was increased with the decrease in the optical energy band gap. The optical constants such as extinction coefficient and refractive index were determined. The intensity of the photoluminescence emission was observed at 398 nm for doped films. The resistivity decreased with the increasing carrier concentration and Hall mobility. The incorporation of Sn into TiO_2 matrix yielded a well-pronounced antibacterial activity for *Bacillus subtilis*.

Keywords Sn-doped TiO_2 thin films · Porous film · Electrical properties and antibacterial activity

✉ A. Arunachalam
mailtoarunachalam88@gmail.com

[1] Department of Physics, Annamalai University, Annamalai Nagar 608 002, Tamil Nadu, India

Introduction

Transparent conducting oxide (TCO) materials are of great interest due to their distinctive physical, chemical, optical and optoelectronic properties. Various TCO materials are ZnO, CdO, SnO, SnO_2 and TiO_2. Among these materials, TiO_2 plays a most promising role in several areas of research because of its high efficient photocatalytic activity, high refractive index, resistance to photo corrosion, chemical stability, low cost and non-toxicity (Malliga et al. 2014). Performance of TiO_2 thin films as a photocatalyst for solar cells or gas sensor depends not only on its energy band structure but also on its crystal structure, crystallite size and morphology (Mechiakh et al. 2011). Film thickness is also an important factor that can influence the performance of TiO_2 thin films (Mechiakh et al. 2007). The structure and semiconducting properties of TiO_2 films can be strongly modified by doping with impurities like Ag, Fe, ZnO (Sen et al. 2005). The recent interest in anatase is motivated by its key role in the injection process in a photochemical solar cell with a high conversion efficiency (Tang et al. 1994). Nanocrystalline TiO_2 thin films are being used as n type electrode in dye-sensitized photoelectrochemical solar cells and as a promising material for quantum dot-sensitized solar cells (Senthil et al. 2010). Another importance of TiO_2 in recent years is the specialization of self-sterilizing surfaces and their implementation in hospitals because of its most reliable and stable under irradiation (Svetlana Nikobuna Pleskova et al. 2012). TiO_2 thin films have been deposited in the past by many research workers using different techniques such as sputtering (Jamuna-Thevi et al. 2011), sol–gel (Mechiakh et al. 2011), pulse laser deposition (Fotsa Ngaffo et al. 2007), chemical bath deposition (Manurung et al. 2013) and spray pyrolysis technique (Weng et al. 2005). Among these

techniques, the spray pyrolysis technique is economic, very simple and suitable for large area thin film preparation.

In this work, we have prepared pristine TiO_2 and Sn-doped TiO_2 thin films and deposited on glass substrates by spray pyrolysis technique. The properties of structural, optical and electrical along with the morphological studies are tuned in such a way for the applications like fabrication of DSSC and for antibacterial activity.

Experimental procedure

TiO_2: Sn thin films were obtained by spray pyrolyzing the precursor solution Titanyl acetylacetonate in air atmosphere in which the atomic ratio of Sn precursor was varied from 0, 2, 4, 6 and 8 at.%. The substrates were well cleaned by the soap solution followed by HCL, acetone and distilled water. Finally, the well-cleaned substrates were dried in an oven. The experimental setup used for the spraying process consists of a spray head and heater, which was kept inside a chamber having an exhaust fan which could remove the gaseous by-products and solvent vapor. The substrate temperature was achieved with the help of automatic temperature controller with an accuracy of ±5 °C. The equal growth of the film was obtained by moving the spray head in the *X–Y* direction which was able to scan an area of 200 × 200 m at a speed of 20 mm^{-1} s^{-1} and in steps of 5 mm^{-1} s^{-1} in the *X–Y* plane direction, respectively. In this unit, the flow rate of the solution was controlled by a stepper motor attached to the solution container. The carrier gas used in this experiment was air. The pressure of the carrier gas was maintained with the help of mechanical gauge. The entire unit was connected to the computer with the help of a serial port. The spray parameters were stored in the computer. Tin-doped TiO_2 films were prepared using (Titanyl acetylacetonate) of 0.1 M and dissolved in ethanol. The doping was achieved by the addition of Tin chloride ($SnCl_4 \cdot 5H_2O$) in at.% (2, 4, 6 and 8 at.%) to the spraying solution, and the whole mixture was sprayed on the glass substrate. The grown films were annealed at 500 °C in the air.

The structural characterization of the deposited films was carried out by X-ray diffraction technique on SHIMADZU-6000 (monochromatic Cu-Kα radiation, $\lambda = 1.5406$ Å). The XRD patterns were recorded in 2θ interval from 10° to 90° with the steps of 0.05° at room temperature. The surface morphology was studied using scanning electron microscopy (SEM) (JEOL-JES-1600) with a magnification of 5000–10,000 μm. The surface topological studies were carried out using Atomic Force Microscope (Nano surf Easy scan2) AGILENT-N9410A-5500. Optical absorption spectrum was recorded in the range of 300–1200 nm using JASCO V-670 spectrophotometer. The photoluminescence spectrum (PL) was studied at room temperature using prolog 3-HORIBAJOBINYVON with an excitation source wavelength of 375 nm. The electrical resistivity, carrier concentration and mobility were measured by automated Hall Effect measurement (ECOPIA HMS—2000 version 2.0) at room temperature in a van der Pauw (VDP) four-point probe configuration.

Antibacterial activity

Preparation of test solution and disc

The test solution was prepared with a known weight of fractions in 10 mg/mL and dissolved in 5 % dimethyl sulphoxide (DMSO). Sterile discs (6 mm) from Himedia Ltd., Mumbai were impregnated with 20 μL of the TiO_2 and Sn-doped TiO_2 (corresponding to 100, 200 and 300 mg/mL) was allowed to dry at room temperature.

Disc diffusion method

The agar diffusion method (Bauer et al. 1966) was followed for antibacterial susceptibility test. Petri plates were prepared by pouring 20 mL of Mueller–Hinton Agar and allowed to solidify for use in susceptibility test against bacteria, respectively. Plates were dried and 0.1 mL of standardized inoculums suspension was poured and uniformly spread. The excess inoculums were drained and the plates were allowed to dry for 5 min. After drying, the discs with TiO_2 and Sn-doped TiO_2 were placed on the surface of the plate with sterile forceps and gently pressed to ensure the contact with the agar surface. Gentamycin (30 mg/disc) was used as the positive control and 5 percent DMSO was used as blind control in these assays. Finally, the inoculated plates were incubated at 37 °C for 24 h. The zone of inhibition was observed and measured in millimeters.

Results and discussion

Structural analysis

X-ray diffraction patterns of tin-doped titanium dioxide thin films are shown in Fig. 1. The films are polycrystalline and fit well with the tetragonal crystal structure. The thin films have anatase phase. The diffraction peak from the XRD pattern is in agreement with the JCPDS card no 21-1272. At 2 at.% of Sn, the intensity of (101) plane decreases which may be due to the decrease in the mobility of titanium and oxygen atoms which lead to the reduction in the nucleation of crystallization phase of anatase TiO_2

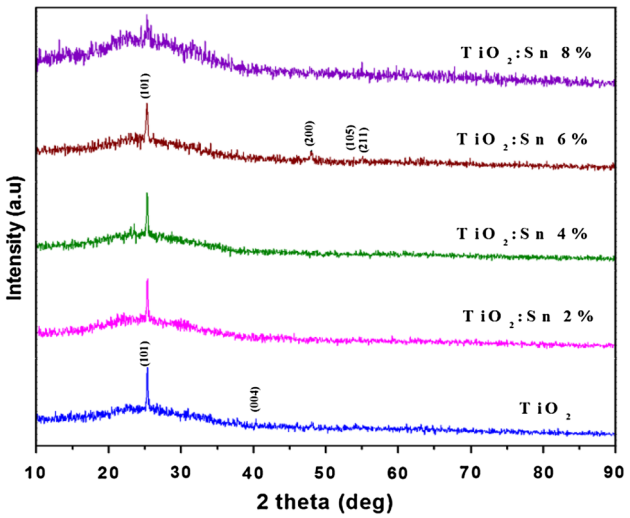

Fig. 1 The XRD pattern of pure TiO_2 and Sn-doped TiO_2 films deposited at the substrate temperature 450 °C

(Abdollahi Nejand et al. 2010). Whereas at 4 at.%, the intensity of (101) plane is again increased which may be due to the presence of Sn^{4+} into TiO_2 lattice structure, leading to the stabilization effect on the crystalline structure of anatase TiO_2 (Huang et al. 2012). The intensity of peak (101) plane increases along with the appearance of other anatase peaks related to (200) and (004) planes with a low intensity of the film deposited with 6 at.% of Sn doping, which indicates that the Ti and O atoms are accommodated easily along (101) plane and this may be due to the influence of Sn atoms. The similar trend was observed by (Huang et al. 2012). The anatase peaks become weak for 8 at.% of Sn concentration which may be due to the reorientation effect (Xu et al. 2010).

The crystallite size (D) is calculated from Scherer's formula (Malliga et al. 2014). From Table 1, the crystallite sizes decrease with increase in Sn content which is attributed to the stress produced by the ionic difference of Sn^{4+} (0.71 nm) and Ti^{4+} (0.68 nm) Chauhan et al. 2012) and also may be due to the increase in Sn–Ti–O bonds in the samples which declines the growth of crystallite sizes (Huang et al. 2012; Caglar et al. 2012). The increase in anatase phase with decrease in crystallite size is favorable to the application such as photodegradation (Li et al. 2013).

The lattice strain (ε) is calculated using the relation

$$\varepsilon = \beta\cos\theta/4 \quad (1)$$

The dislocation density is defined as the length of dislocation lines per unit volume of the crystal was estimated from the following relation using the simple approach of Williamson and Smallman (Pan et al. 2013).

The value of dislocation density (δ) is calculated using the relation:

$$\delta = 1/D^2 \quad (2)$$

It is observed that as the doping concentration increases, the dislocation density is increased because of the difference in ionic radii of Ti^{4+} and Sn^{4+}.

The microstress of the prepared films is calculated using

$$\sigma_{\text{stress}} = \varepsilon/2E \quad (3)$$

where E is the Young's modulus of the material (282.76 GPa), and ε is the strain of the film (Moses Ezhil Raj et al. 2010). The obtained negative value indicates that the stress is in compressive nature. The observed stress slightly increases, which is due to the change in the morphology of the film while doping concentration increased Prasada Rao et al. 2010). The texture coefficient (TC) references the texture of a particular plane, whose deviation from unity implies the preferred growth. Quantitative information concerning the preferential crystallite orientation is obtained from different $TC_{(hkl)}$ defined by the well-known relation (Al-Obaidi et al. 2013).

$$TC_{(hkl)} = \left(I_{(hkl)}/I_{0(hkl)}\right)/N^{-1}\Sigma_n\left(I_{(hkl)}/I_{0(hkl)}\right) \quad (4)$$

where $TC_{(hkl)}$ is the texture coefficient, $I_{(hkl)}$ is the XRD intensity, N is the reflection number and n is number of diffraction peaks considered. $I_{0(hkl)}$ is the intensity of the XRD reference of the standard diffraction peaks. The

Table 1 Variation of crystallite size (D), dislocation density (δ), strain (ε), stress (σ_{stress}), texture coefficient (TC) and lattice parameters (a and c) for pure TiO_2 and Sn-doped TiO_2 thin films

at.% of Sn	$D \times 10^{-9}$ (m)	$\varepsilon \times 10^{-3}$	$\delta \times 10^{14}$ (lines/m)	σ_{stress} (GPa)	TC	Lattice constant (Å)	
						a	c
0	17.09	2.0279	34.2301	−4.3969	1.6755	3.7466	9.5056
2	14.35	3.3663	48.5524	−0.5139	1.7579	3.7574	9.5128
4	16.31	2.1251	37.5917	−0.5384	1.1558	3.7578	9.5122
6	13.83	2.5052	52.2824	−0.5292	1.0110	3.7715	9.5116
8	13.57	2.5531	54.3050	−0.5139	1.1080	3.7772	9.5112

texture coefficient of the films is higher than 1 which indicates abundance orientation of the crystallites along (101) plane. But at higher doping concentration of Sn, the texture coefficient is much lesser than 1, and it indicates the absence of orientation (Al-Obaidi et al. 2013). The increased texture coefficient ($TC_{(hkl)} > 1$) of the undoped film shows the preferential orientation of the crystallites along (101) plane. The observed $TC_{(hkl)} \sim 1$ for the film deposited with 4 and 6 at.% of Sn shows the change of preferential orientation to random (Mariappan et al. 2012).

$$\frac{1}{d^2} = \frac{h^2 + k^2}{a^2} + \frac{l^2}{c^2} \quad (5)$$

The lattice constants calculated for TiO_2 thin films are shown in Table 1. The 'a' and 'c' values are in concordance with the standard values of TiO_2 single crystals ($a = 3.785$ nm and $c = 9.513$ nm); these indicate that the quality of TiO_2 films is good crystalline in nature. The lattice parameter of the doped films a and c is less than the bulk value which is a strong indication of stress in the films. It is noted that the lattice constant 'c' is decreased, but the lattice constant 'a' is increased significantly and less than the bulk value which is attributed to the difference in the ionic radius of Sn^{4+} and Ti^{4+} (Chauhan et al. 2012; Muiva et al. 2011; Tu et al. 2009).

Morphological studies

Surface morphology

The morphology of the thin films is analyzed by scanning electron microscopy. Figure 2 shows the SEM micrographs of pristine TiO_2 and Sn-doped TiO_2 thin films on glass substrate deposited at optimized temperature 450 °C. It is observed that the morphology of the films strongly depends on the concentration of dopants. The morphology of TiO_2 films and 2 at.% of Sn-doped TiO_2 films depict the uniform distribution of grains covering the entire surface area of the substrate. For the doping concentration of 4 at.% of Sn, the film exhibits the distribution of spherical grains with porous nature. The film doped with 6 at.% of tin is suitable for fabrication of DSSC because it exhibits uniform distribution of spherical grains with large in size, also with the porous nature of the film. The porous films play an interesting role in DSSC in enhancing dye-sensitization when these TiO_2 films are used in solar cell application (Manurung et al. 2013; Allah et al. 2007). However, at higher doping concentration (8 at.%), the growth of grains is suppressed and segregated due to the presence of compressive stress in the film and it is in agreement with the XRD results. Figure 2f, g, h, i, j shows SEM images of TiO_2 surface occupancy plot of Sn-doped TiO_2 thin film using software analysis.

Composition of the films is studied by EDAX analysis in Fig. 3a, b. In Fig. 3a, the spectrum depicts the presence of Ti and O. The spectrum in Fig. 3b evidences the presence of Sn along with Ti and O.

Surface topography

Atomic force microscopy (AFM) images of pure and doped thin films are shown in Fig. 4a, b. The pure TiO_2 film (Fig. 4a) reveals the uniform distribution of spherical-shaped grains. Flake-like structure covered the entire surface. This may be due to increments of metal nucleation centers, which resulted in the particle growth. The doped film (Fig. 4b) depicts polycrystalline nature with uniform distribution of pyramidal-shaped grains and shows voids-free surface. The observed columnar grains in 3D image show the growth along the (101) direction for the undoped TiO_2 and is in agreement with the XRD results. The surface roughness of undoped and doped films is found to be 16 and 29 nm, respectively. The dye molecules that fill the pores absorb the incident radiation and inject electrons into the conduction band of the TiO_2 semiconductor easily and hence enhances the performance of the solar cell (Fotsa Ngaffo et al. 2007). The increase in the particle size and surface roughness for the doped films evidenced that it contributes in enhancing the large surface for the absorption of more dye molecules which act as an active sensitizer to enhance the efficiency of the DSSCs. The 3D image of Fig. 4b exhibits the sharp peaks, shows the growth along the (101) direction for the Sn-doped TiO_2 film and is in agreement with the XRD results. Figure 4c, d exhibits plot profile and selected area using software analysis.

Optical properties

Transmittance

Figure 5 shows the optical transmittance spectra of the pure and Sn-doped TiO_2 thin films in the wavelength range of 300–1200 nm. The optical transmittance of pure and doped films is above 75 % in the visible region. As doping concentration increases, the transmittance of the doped film enhances up to 85 % for 6 at.% and decreases to 8 at.% of tin. First the enhancement of the transmittance might be attributed to the well crystallization of the film. The high transparency of the films is associated with a good structural homogeneity and crystallinity (Shinde et al. 2013). The film with transmittance higher than 85 % is suitable for photovoltaic applications (Liu et al. 2012). At higher doping concentration of the tin, the scattering of photons increases due to increased crystal defects and hence the transmittance decreases (Weng et al. 2005).

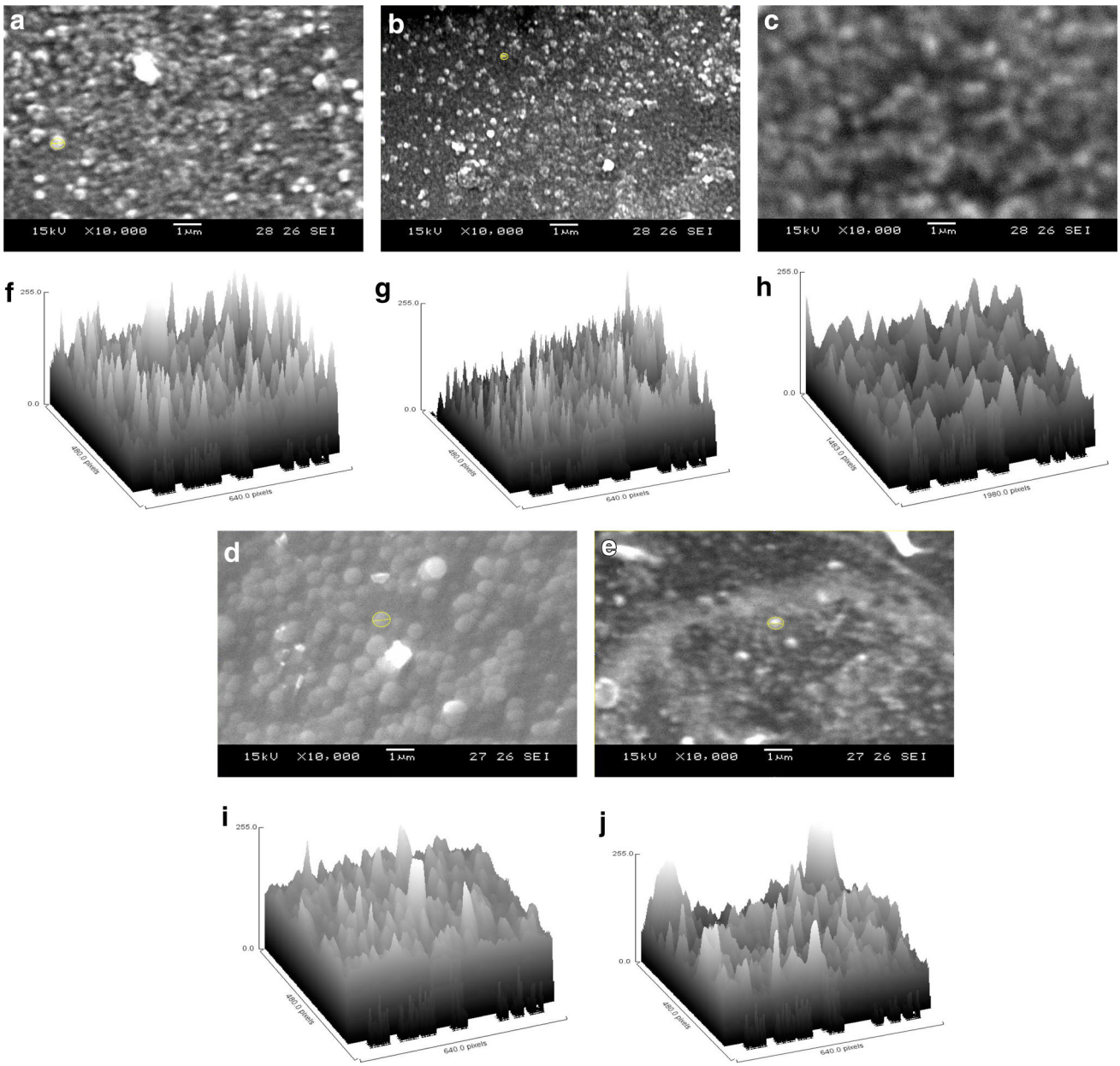

Fig. 2 SEM micrographs for the **a** undoped TiO_2, **b** 2 at.%, **c** 4 at.%, **d** 6 at.% and **e** 8 at.% of Sn-doped TiO_2 films, **f** undoped TiO_2, **g** 2 at.%, **h** 4 at.%, **i** 6 at.% and **j** 8 at.% surface occupancy plot of Sn-doped TiO_2 thin film

Optical band gap

The band gap energy of TiO_2 can be determined from a plot of $(\alpha hv)^{1/2}$ versus energy (hv), as shown in Fig. 6

$$\alpha hv = A\left(hv - E_g\right)^n \quad (6)$$

where A is a constant, and E_g is the band gap value. E_g can be determined by extrapolating the straight line portion at $\alpha = 0$ as seen in Fig. 6.

The band gap of the semiconductor material is closely related to the wavelength absorbed; the wavelength of the light absorbed increases with decrease in the band gap. Figure 6 shows the energy band gap for pure and Sn-doped TiO_2 thin films. It is observed that the band gap of the material decreases from 3.5 to 2.79 eV with increase in Sn concentration, which indicates the improvement in the minimum energy required for excitation electron. The electron can easily be excited from the valence band to conduction band (Firdaus et al. 2012). The band gap of the observed film is much higher than the bulk value of TiO_2 (3.2 eV) indicating the formation of nanosized grains. The decrease in the band gap of the doped films is attributed to

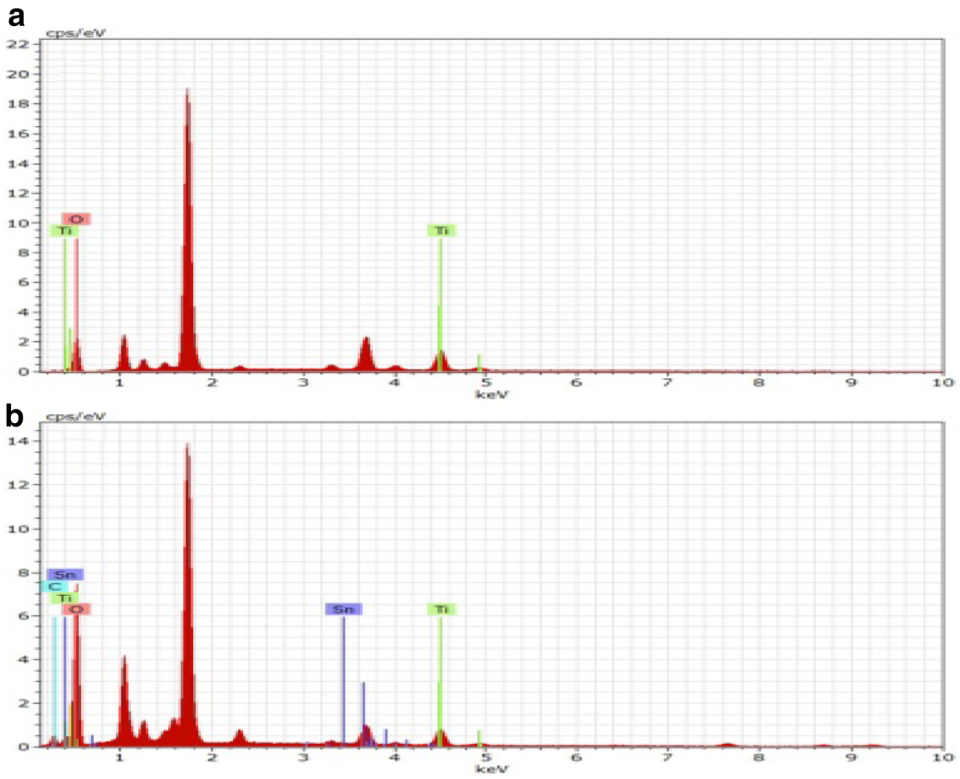

Fig. 3 EDAX spectrum of pure TiO_2 and 6 at.% Sn-doped TiO_2 thin films

be a promising material for a potential application for TiO_2-based materials such as in the fabrication of DSSC (Weng et al. 2005; Li et al. 2013).

Extinction coefficient and refractive index

The extinction coefficient of TiO_2 thin film has been calculated from

$$k = \frac{\alpha\lambda}{4\pi} \tag{7}$$

$$n = \frac{1 + R^{1/2}}{1 - R^{1/2}} \tag{8}$$

From Fig. 7, it is observed that the extinction coefficient is decreased as the wavelength is increased and this shows the qualitative indication of surface smoothness and homogeneity of the sprayed films (Shanmuganathan et al. 2013).

Figure 8 represents the refractive index of the films which is slightly higher than bulk anatase (2.52). At higher wavelength, the refractive index begins to decrease and reaches a constant level which may be due to the presence of high porosity in these films (Tripra Sundari et al. 2011). The refractive index of the doped film shows the variation up to 2.65 in the visible region which is preferred for antireflection coating materials in the window layers of the solar cell (Allah et al. 2007).

Photoluminescence (PL)

Photoluminescence emission spectra are useful to understand the fate of electron–hole pairs in semiconductor particles (Yamashita et al. 2003) (Figs. 9, 10). The intensity of the photoluminescence spectrum of the pristine TiO_2 film is much higher than the doped TiO_2 film at 398 nm. The reduction of photoluminescence intensity with the increase in dopant concentration indicates the retardation of recombination process which is probably due to the efficient transfer of charge into highly dispersed nanosized Sn (Yang et al. 2009) and higher photocatalytic activity of doped film can be obtained due to the lower recombination of electron and hole (Li et al. 2013). With the increasing Sn^{4+} concentration, the photoluminescence intensity decreases. A decrease in the photoluminescence intensity indicates a lower recombination rate of electron–hole pairs and hence higher separation efficiency (Yadava et al. 2014).

Electrical properties

The electrical properties such as resistivity, mobility and carrier concentration are carried out at room temperature by Hall Effect measurement and are tabulated in Table 2. It is observed that as the Sn content increases, the resistivity decreases with the increase in carrier concentration and Hall mobility.

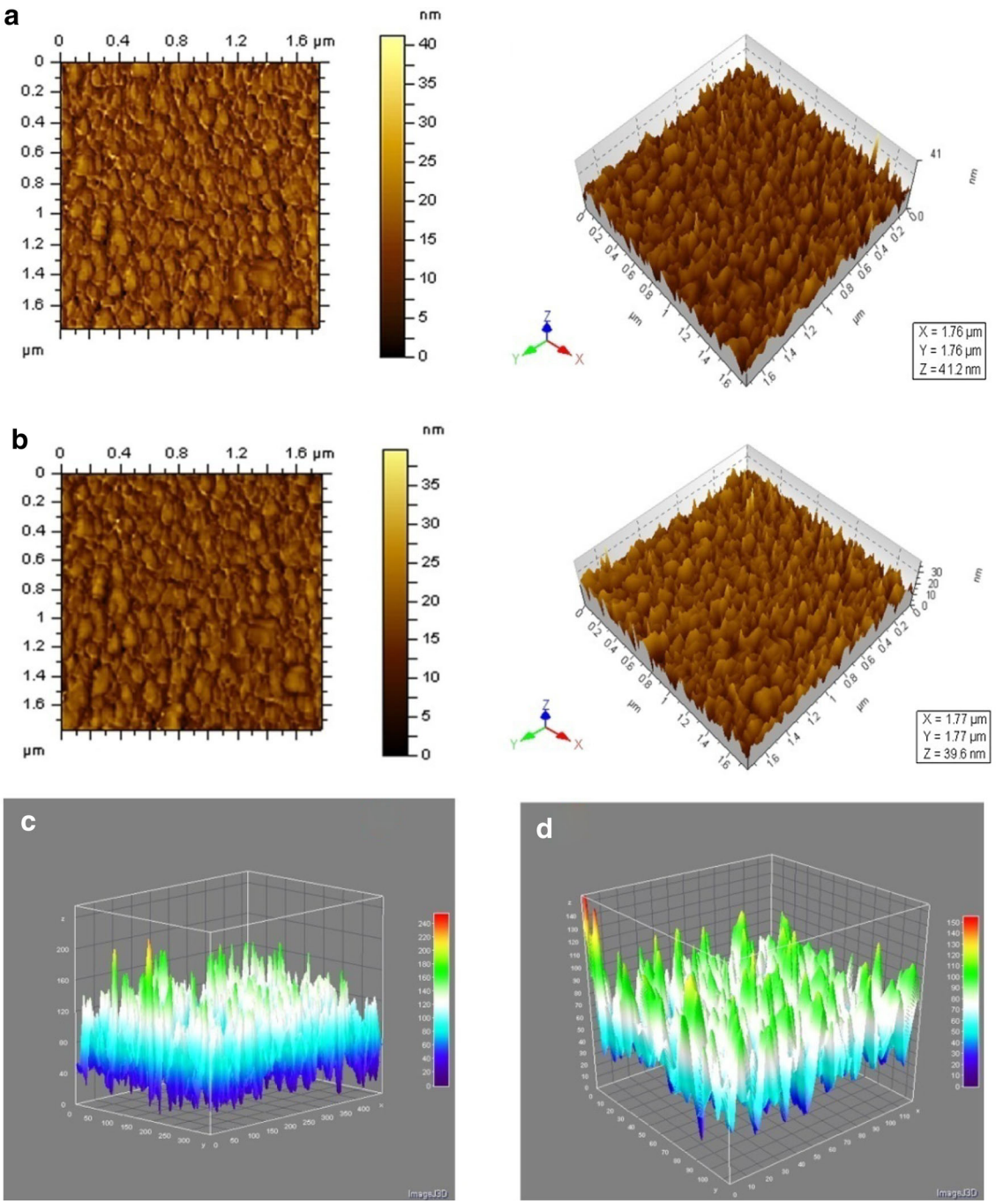

Fig. 4 AFM micrographs for **a** undoped TiO_2 and **b** Sn-doped (6 at.%) TiO_2 films **c** undoped TiO_2 and **d** Sn-doped TiO_2 (6 at.%) surface plot of thin films

It is attributed to the substitution of Sn^{4+} in Ti^{4+} sites of TiO_2, which gives two more free electrons to contribute to the electrical conductivity. According to the morphological studies, the film exhibits the porous nature with homogeneity and the grains exhibit absence of closed packed morphology which results in the weak carrier scattering process resulted in increase in mobility (Firdaus et al. 2012). But at higher doping of Sn, the resistivity increases with the decrease in carrier concentration and Hall mobility. This is attributed to the excess of tin atoms which might not occupy the correct places inside the TiO_2 lattice because the excess of Sn may occupy the interstitial positions and distort the crystal structure as seen in the XRD results (Fig. 1), which may negatively affect the electronic

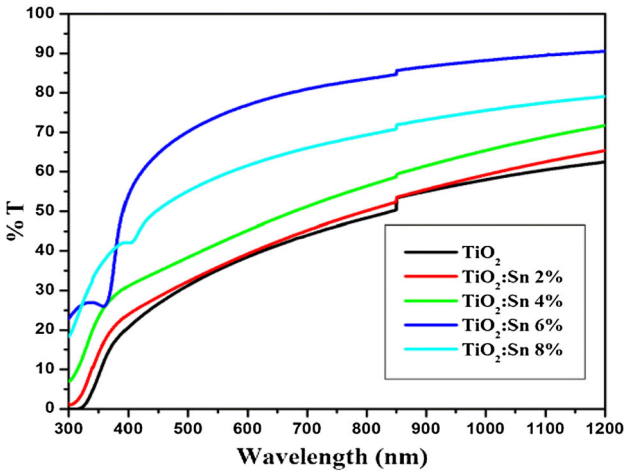

Fig. 5 Optical transmittance of Sn-doped TiO_2 thin films

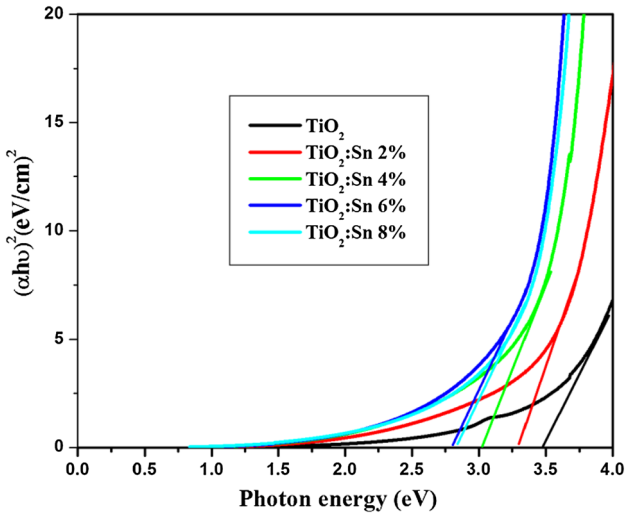

Fig. 6 Variation of $(\alpha h\nu)^2$ vs $h\nu$ of the Sn-doped TiO_2 thin films

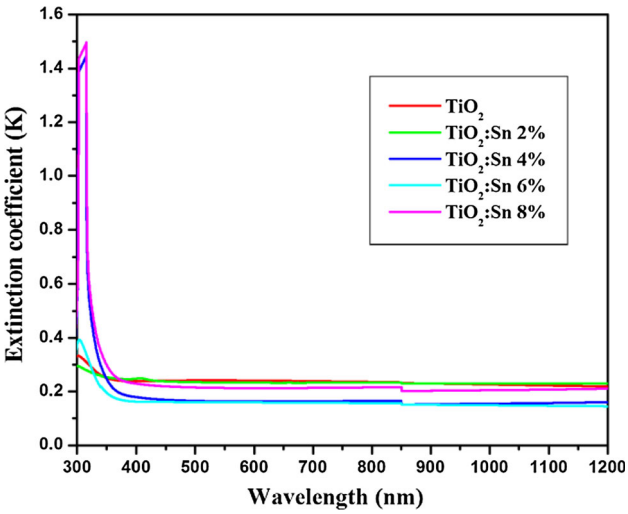

Fig. 7 The variation of extinction coefficient of the TiO_2 and Sn-doped TiO_2 thin films with wavelength

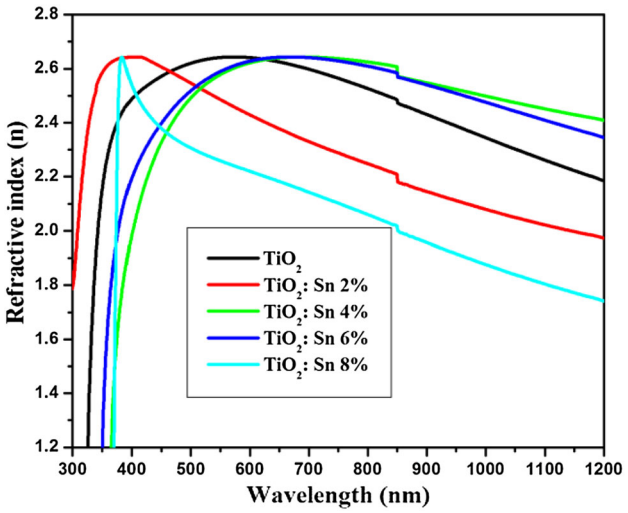

Fig. 8 The variation of refractive index of the TiO_2 and Sn-doped TiO_2 thin films with wavelength

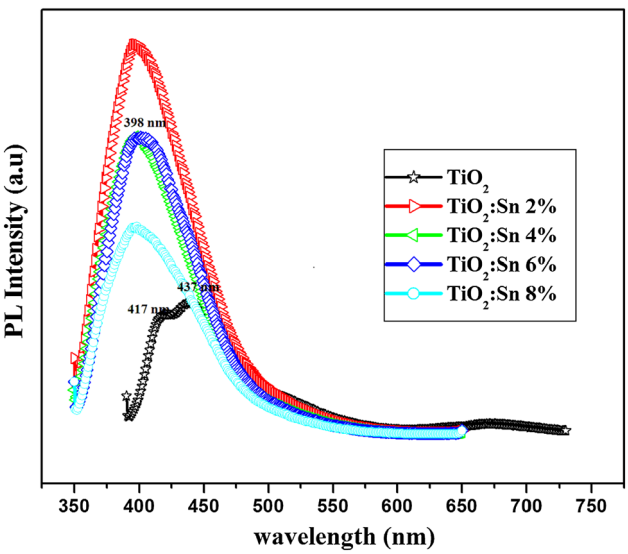

Fig. 9 Photoluminescence emission spectra for undoped and Sn-doped TiO_2 films prepared at 450 °C

mobility. Therefore, the disorder is produced in the lattice, and thus increases the efficiency of scattering mechanism such as phonon scattering and ionized scattering which in turn cause increase in resistivity (Caglar et al. 2012).

Antibacterial activity

Generally, TiO_2 is known for its chemical stability and optical competency. It has been used extensively for killing different groups of microorganisms including bacteria, fungi and viruses, because it has high photoreactivity, broad-spectrum antibiosis and chemical stability. Therefore, pure TiO_2 and 6 at.% of Sn-doped TiO_2 are taken for

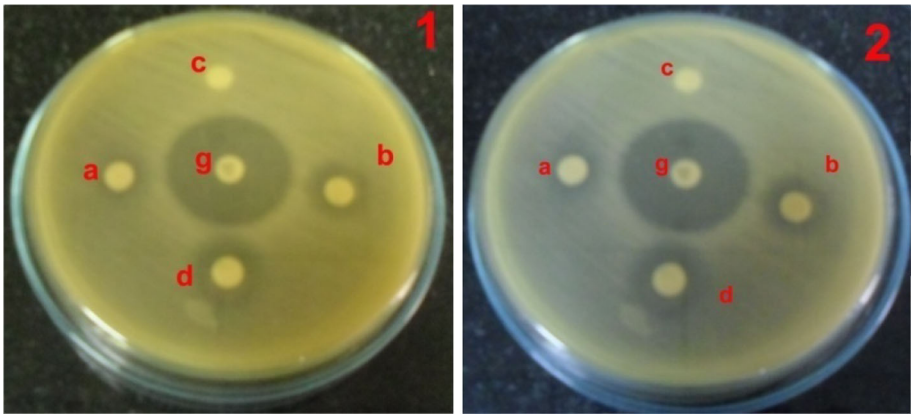

Fig. 10 Antibacterial activity on **1** pure TiO_2 **2** 6 at.% of Sn-doped TiO_2 films, *g* positive control, *c* negative control, *a* 100 mg/mL, *b* 200 mg/mL, *d* 300 mg/mL

Table 2 Electrical properties of pure TiO_2 and 6 at.% of Sn-doped TiO_2 thin films

Sample	Resistivity (Ω-cm)	Mobility (Cm^2/Vs)	Carrier concentration (cm^{-3})
TiO_2	1.37×10^{-3}	39.32×10^{21}	1.55×10^{20}
6 at.% Sn–TiO_2	1.19×10^{-3}	44.76×10^{21}	11.15×10^{20}

Table 3 Antibacterial activity of TiO_2 film

Organisms	Control	Gentamycin 30 mg	Zone of inhibition (mg/mL)		
			100	200	300
Staphylococcus aureus	NZ	29	NZ	NZ	NZ
Klebsiella pneumonia	NZ	18	NZ	NZ	11
Pseudomonas aeruginosa	NZ	13	8	9	11
Proteus mirabilis	NZ	21	NZ	NZ	NZ
Bacillus subtilis	NZ	21	11	13	15

antibacterial activity and tested with five bacteria, namely *Staphylococcus aureus*, *Klebsiella pneumonia*, *Pseudomonas aeruginosa*, *Proteus mirabilis* and *Bacillus subtilis*.

The antibacterial activity of pure TiO_2 in different concentrations against bacteria (*S. aureus*, *K. pneumonia*, *P. aeruginosa*, *P. mirabilis* and *B. subtilis*) is observed. The mean zone of inhibition is ranged between 11 and 15 mm. Gentamycin is a positive control; the zone of inhibition is ranged from 13 to 29 mm, respectively. The highest mean zone of inhibition (15 mm) is recorded *Bacillus subtilis* with against pure TiO_2 presented in Table 3.

The antibacterial activity of Sn-doped TiO_2 with 6 at.% in different concentrations against bacteria (*Staphylococcus aureus*, *Klebsiella pneumonia*, *Pseudomonas aeruginosa*, *Proteus mirabilis* and *Bacillus subtilis*) is noted. The mean zone of inhibition is ranged between 10.5 and 18 mm. Gentamycin is a positive control; the zone of inhibition is ranged from 13 to 29 mm respectively. The highest mean zone of inhibition (18 mm) is recorded *Bacillus subtilis* with against Sn-doped TiO_2 with 6 at.% presented in Table 4. Overall, 6 at.% Sn-doped TiO_2 with coatings has good antibacterial property which entitles them to be used as antibacterial surface coatings in biomedical applications. The similar study was studied Ag-doped TiO_2 (Jamuna-Thevi et al. 2011).

Table 4 Antibacterial activity of Sn-doped TiO_2 film

Organisms	Control	Gentamycin 30 mg	Zone of inhibition (mg/mL)		
			100	200	300
Staphylococcus aureus	NZ	29	NZ	NZ	9
Klebsiella pneumonia	NZ	18	NZ	8.5	9.5
Pseudomonas aeruginosa	NZ	13	NZ	NZ	NZ
Proteus mirabilis	NZ	21	NZ	NZ	NZ
Bacillus subtilis	NZ	21	10.5	13	18

Conclusion

XRD pattern of the deposited films (TiO_2 and Sn-doped TiO_2) revealed the tetragonal structure with preferential orientation along (101) plane. The SEM study evidenced the nanosized grains with the porous nature for 6 at.% of Sn-doped TiO_2 film. The increased particle size and surface roughness value were noticed in AFM for 6 at.% Sn-doped films. The enhanced transmittance and decrease in band gap were due to Sn dopant. The PL intensity was decreased with increase in dopant and it was attributed to the retardation of recombination process. The resistivity was decreased with increase in the mobility and carrier concentration. Therefore, from the above characterizations, it is confirmed that 6 at.% Sn-doped TiO_2 is suitable for the fabrication DSSC when it is deposited on ITO-coated glass plate as a photoelectrode. Also the incorporation of Sn into

the TiO_2 matrix yields a well-pronounced antibacterial activity than the pure TiO_2 film.

Acknowledgments The authors thank the UGC Minor Project, New Delhi, India, for the financial support through research Grant no. 41-1398/2012(SR).

References

Abdollahi Nejand B, Sanjabi S, Ahmadi V (2010) Optical and photocatalytic characteristics of nitrogen doped TiO_2 thin film deposited by magnetron sputtering. Trans F Nanotechnol (Sharif University of Technology) 17:102–107

Allah FK, Abe SY, Nu nez CM, Khelil A, Cattin L, Morsli M, Berne'de JC, Bougrine A, Del Valle MA, Daz FR (2007) Characterisation of porous doped ZnO thin films deposited by spray pyrolysis technique. Appl Surf Sci 253:9241–9247

Al-Obaidi SS, Yousif AA, Al-Haitham I (2013) Synthesis of nanostructured TiO2 thin films by pulsed laser deposition (PLD) and the effect of annealing temperature on structural and morphological properties. J Pure Appl Sci 26

Bauer AW, Kirby WMM, Sherris JC, Turck M (1966) Antibiotic susceptibility testing by a standardized single disk method. Am J Clin Phathol 45:493–496

Caglar Y, Caglar M, Ilican S (2012) Microstructural, optical and electrical studies on sol gel derived ZnO and ZnO: Al films. Curr Appl Phys 12:963–968

Chauhan R, Kumar A, Chaudhary RP (2012) Structural and optical characterization of Zn doped TiO2 nano particles prepared by sol–gel method. J Sol-Gel Sci Technol 61:585–591

Firdaus CM, Shah Rizam MSB, Rusop M, Rahmatul Hidayah S (2012) Characterization of ZnO and ZnO: TiO_2 thin films prepared by sol–gel spray—spin coating technique. Procedia Eng 41:1367–1373

Fotsa Ngaffo F, Caricato AP, Fernandez M, Martino M, Romano F (2007) Structural properties of single and multilayer ITO and TiO_2 films deposited by reactive pulse laser ablation deposition technique. Appl Surf Sci 253:6508–6651

Huang F, Li Q, Thorogood GJ, Cheng YB, Caruso RA (2012) Zn doped TiO_2 electrodes in dye-sensitized solar cells for enhanced photocurrent. J Mater Chem 22:17128–17132

Jamuna-Thevi K, Bakar SA, Ibrahim S, Shahab N, Toff MRM (2011) Quantification of silver ion release, in vitro cytotoxicity and antibacterial properties of nanostuctured Ag doped TiO_2 coatings on stainless steel deposited by RF magnetron sputtering. Vacuum 86:235–241

Li F, Guan LX, Dai ML, Feng JJ, Yao MM (2013) Effects of V and Zn codoping on the microstructures and photocatalytic activities of nanocrystalline TiO2 films. Ceram Inter 39:7395–7400

Liu J, Ma SY, Huang XL, Ma LG, Li FM, Yang FC, Zhang Q, Zhao Q, Zhang XL (2012) Effect of Ti-doped concentration on the microstructures and optical properties of ZnO thin films. Superlattices Microstruct 52:765–773

Malliga P, Pandiarajan J, Prithivikumaran N, Neyvasagam K (2014) Influence of film thickness on structural and optical properties of sol–gel spin coated TiO_2 thin film. J Appl Phys 6:22–28

Manurung P, Putri Y, Simanjuntak W, Lowc IM (2013) Synthesis and characterisation of chemical bath deposited TiO_2 thin-films. Ceram Int 39:255–259

Mariappan R, Ponnuswamy V, Suresh P (2012) Effect of doping concentration on the structural and optical properties of pure and tin doped zinc oxide thin films by nebulizer spray pyrolysis (NSP) technique. Superlattices Microstruct 52:500–513

Mechiakh R, Meriche F, Kremer R, Bensaha R, Boudine B, Boudrioua A (2007) TiO_2 thin films prepared by sol–gel method for wave guiding applications: Correlation between the structural and optical properties. Opt Mater 30:645–651

Mechiakh R, Ben Sedrine N, Chtourou R (2011) Sol–gel synthesis, characterization and optical properties of mercury-doped TiO_2 thin films deposited on ITO glass substrates. Appl Surf Sci 257:9103–9109

Moses Ezhil Raj A, Agnes V, Bena Jothy V, Ravidhas C, Wollschlager J, Suendorf M, Neumann M, Jayachandran M, Sanjeeviraja C (2010) Spray deposition and property analysis of anatase phase titania (TiO_2) nanostructures. Thin Solids Films 519:129–135

Muiva CM, Sathiaraj TS, Maabong K (2011) Effect of doping concentration on the properties of aluminum doped zinc oxide thin films prepared by spray pyrolysis for transparent electrode applications. Ceram Int 37:555–560

Pan Z, Zhang P, Tian X, Cheng G, Xie Y, Zhang H, Zeng X, Xiao C, Hu G, Wei Z (2013) Properties of fluorine and tin co-doped ZnO thin films deposited by sol–gel method. J Alloys Compd 576:31–37

Pleskova SN, Golubeva IS, Verevkin YK (2012) Dynamics to the TiO_2 nanofilms bactericidal activity. J Environ Occup Sci 1:71–76

Prasada Rao T, Santhosh Kumar MC, Safarulla A, Ganesan V, Barman SR, Sanjeeviraja C (2010) Physical properties of ZnO thin films deposited at various substrate temperatures using spray pyrolysis. Phys B 405:2226–2231

Sen S, Mahanty S, Roy S, Heintz O, Bourgeois S, Chaumont D (2005) Investigation on sol–gel synthesized Ag-doped TiO_2 cermet thin films. Thin Solid Films 474:245–249

Senthil TS, Muthukumarasamy N, Agilan S, Thambidurai M, Balasundaraprabhu R (2010) Preparation and characterization of nanocrystalline TiO_2 thin films. Mater Sci Eng B 174:102–104

Shanmuganathan G, Shameem Banu IB, Krishnan S, Ranganathan B (2013) Influence of K-Doping on the optical properties of ZnO thin films grown by chemical bath deposition method. J Alloy Compd 562:187–193

Shinde SS, Korade AP, Bhosale CH, Rajpure KY (2013) Influence of tin doping onto structural morphological, optoelectronic and impedance properties of sprayed ZnO thin films. J Alloy Compd 551:688–693

Tang H, Prasad K, Sanjinès R, Schmid PE, Lévy F (1994) Electrical and optical properties of TiO_2 anatase thin films. J Appl Phys 75:2042

Tripra Sundari S, Raut NC, Mathews Tom, Ajikumar PK, Dash S, Tyagi AK, Raj Baldev (2011) Ellipsometric studies on TiO_2 thin films synthesized by spray pyrolysis technique. Appl Surf Sci 257:7399–7404

Tu YF, Huang SY, Sang JP, Zou XW (2009) Synthesis and photocatalytic properties of Sn-doped TiO2 nanotube arrays. J Alloys Compd 482:382–387

Weng W, Ma M, Du P, Zhao G, Shen G, Wang J, Han G (2005) Superhydrophilic Fe doped titanium dioxide thin films prepared by a spray pyrolysis deposition. Surf Coat Technol 198:340–344

Xu L, Shen H, Zhu R (2010) Influence of annealing temperature on the photoluminescence property of ZnO thin film covered by TiO_2 nanoparticles. J Lumin 130:2123–2127

Yadava HM, Otaria SV, Kolia VB, Mali SS, Hong CK, Pawara SH, Delekara SD (2014) Preparation and characterization of copper-doped anatase TiO2 nanoparticles with visible light photocatalytic antibacterial activity. J Photochem Photobiol A Chem 280:32–38

Yamashita H, Harada M, Misaka J, Takeuchi M, Neppolian B, Anpo M (2003) Photocatalytic degradation of organic compounds diluted in wate rusing visible light-responsive metal ion-implanted TiO_2 catalysts: Feion-implanted TiO_2. Catal Today 84:191–196

Yang D, Park SE, Lee JK, Lee SW (2009) Sonochemical deposition of nanosized Au on titanium oxides with different surface coverage and their photocatalytic activity. J Cryst Growth 311:508–511